ChemComm

COMMUNICATION

View Article Online
View Journal | View Issue

Cite this: *Chem. Commun.*, 2024, **60**, 12557

Received 7th September 2024,
Accepted 1st October 2024

DOI: 10.1039/d4cc04590d

rsc.li/chemcomm

A local hydroxyl group-modified copper site directs the oxidation of carbon monoxide†

Guoqiang Cao [ab] and Nan Yi *[a]

A washing step is employed to adjust the residual surface hydroxyl groups on the Cu–TiO_2 catalysts, which in turn influences the local environment of copper species. Hydroxyl groups control both copper dispersion and the Cu^+/Cu^{2+} ratio. Notably, a higher $[Cu^+]/[OH^-]$ ratio is associated with an enhanced reaction rate in CO conversion.

Copper oxides, both unsupported or supported by an oxide,[1,2] have been explored as catalysts of carbon monoxide (CO) oxidation. This is because copper exhibits catalytic activity that is comparable to that of precious metals, while available at a much lower cost. Results of studies performed under high vacuum conditions suggested that low valence copper species, notably Cu(I), are highly effective at accelerating the rate of CO oxidation.[3] However, identification of the precise copper oxidation state becomes difficult once the copper is supported by an oxide. This is particularly notable when copper is supported by reducible metal oxides, such as titanium dioxide or cerium oxide.[4–6] The interaction between copper oxides and reducible metal oxides alters the electronic and structural properties of copper metal. Other surface species, including those associated with supports and/or introduced *via* the reactant stream, may also have an impact on CO oxidation due to their capacity to alter the local chemical environment.[7,8] Hydrogen pre-reduction has always been recommended as a means to increase the concentration of Cu(I), which has an impact on the rate of CO conversion.[9,10] Meanwhile, the addition of water (H_2O) vapor in the reactant streams, even at low concentrations, affects the copper-based catalysts intended for use in CO oxidation.[11] The formation of CO–H_2O surface complexes may also block the active sites on the surface. As an H_2O-derived species, the hydroxyl group exhibits varied functions depending on the surface coverage.[12,13] For example, the accumulation of hydroxyl groups inhibited the redox process catalysed by Cu–CeO_2.[14] The presence of hydroxyl groups was suggested to be correlated directly with the formation of surface bicarbonate species by Cu–CeO_2 catalysts.[14]

Traditional approaches to the synthesis of copper-based catalysts include a calcination step. Calcination promotes the formation of copper oxides *via* the thermal decomposition of copper hydroxides. However, thermal post-treatments also reconstruct the surface and lead to changes of critical surface properties. Here, we used a direct approach to synthesise copper oxides supported by titanium dioxides (Cu–TiO_2) *via* a reaction between copper(II) acetate and sodium hydroxide.[15,16] In contrast to other copper precursors, copper(II) acetate facilitates the formation of copper(II) oxide in a single step. The precipitates from this reaction are then washed with deionised H_2O to adjust the concentrations of residual surface hydroxyl groups. Using this simple approach, we can obtain a catalyst that features hydroxyl groups in the immediate vicinity of copper oxide on the catalyst surface. In this study, this platform was used to investigate the impact of surface hydroxyl concentration on the rate of CO oxidation.

The copper weight loading was adjusted to achieve 10 wt%. The precipitates were separated from the parent aqueous solution without additional washing. It is symbolised as Cu–TiO_2-pH14. Cu–TiO_2-pH9 and Cu–TiO_2-pH7 were obtained after further washing of the Cu–TiO_2-pH14 precipitate with deionised water. The suffixes pH9 and pH7 represent the pH values of the final wash solution measured immediately before the precipitates were collected. X-Ray diffraction (XRD) profiles revealed no diffraction peaks that could be attributed to copper oxides (Fig. S1, ESI†). Inductively coupled plasma (ICP) analysis revealed a copper concentration of 9.2 wt%. The surface copper concentration determined by X-ray photoelectron spectroscopy (XPS) was ~6.2 wt% regardless of the number of washing steps. The surface area of the TiO_2 support is 116 m^2 $gcatal^{-1}$. Compared to the undoped TiO_2 support, the addition of copper resulted in an overall decrease in total surface area (Table 1). Meanwhile, the surface area gradually increased as the pH value of the parent solution approached 7. This increase may be explained by the fact that the washing step removes extra sodium hydroxide from the pores of the Cu–TiO_2 catalyst. Therefore, more surface area becomes available after the washing steps.

[a] *Department of Chemical Engineering and Bioengineering, University of New Hampshire, Durham, New Hampshire 03824, USA. E-mail: nan.yi@unh.edu*
[b] *State Key Laboratory of Coal Conversion, Institute of Coal Chemistry, Chinese Academy of Sciences, Taiyuan 030001, P. R. China*

† Electronic supplementary information (ESI) available: Experimental methods, X-ray powder diffraction (XRD) profiles, cyclic light-off curves, IR profiles and XPS spectra. See DOI: https://doi.org/10.1039/d4cc04590d

Table 1 Physical properties and CO conversion rates of Cu–TiO_2 catalysts

Sample	Surface area (m^2 $gcatal^{-1}$)	Copper concentration			
		Cu dispersion[a] (%)	$(Cu^+/Cu^{2+})^b$	$(Cu^+/OH^-)^b$	Reaction rate[c] (μmol s^{-1} $gcatal^{-1}$)
Cu–TiO_2-pH7	108	60.4	30.8	1.10	0.16
Cu–TiO_2-pH9	101	56.4	36.6	1.09	0.06
Cu–TiO_2-pH14	85	48.6	42.3	0.96	0.03

[a] Measured by nitrous oxide (N_2O) absorption. [b] Integrated peak areas based on 932.4 eV for Cu^+, 933.7 eV for Cu^{2+}, and 531.6 eV for OH^-. [c] Measured at 75 °C, 1% carbon monoxide (CO) + 20% oxygen (O_2) balanced with helium; gas hourly space velocity (GHSV), 36 000 h^{-1}.

Cu–TiO_2 catalysts were evaluated for CO oxidation. Results from light-off activity tests revealed that Cu–TiO_2 obtained from aqueous solutions at lower pH values are more effective at catalysing CO conversion (Fig. 1a). The catalytic activity of Cu–TiO_2-pH7 is similar to that of Cu–TiO_2-pH9. Both catalysts achieved a T_{50} (50% CO conversion) at ~125 °C and full CO conversion at reaction temperatures below 200 °C. By contrast, and although Cu–TiO_2-pH7 and Cu–TiO_2-pH14 have the same copper concentration based on ICP and XPS analysis, reactions that included Cu–TiO_2-pH14 achieved only 50% CO conversion at 185 °C. As shown in Table 1, copper dispersion decreases with an increase in the concentration of residual hydroxyl groups. The copper dispersion values for Cu–TiO_2-pH7 and Cu–TiO_2-pH14 catalysts were 60.4% and 48.6%, respectively. Therefore, it suggested that the concentration of surface hydroxyl groups has a direct impact on copper dispersion and the CO conversion. After the first reaction cycle, the samples were cooled to ambient temperature with pure helium, and the activity was re-evaluated with no additional treatment. This cyclic test showed that the light-off curves determined for both Cu–TiO_2-pH7 and Cu–TiO_2-pH14 exhibited the same trend after three runs (Fig. S2, ESI†). Thus, our results suggest that localised hydroxyl groups are stable under the conditions used in these experiments.

To further understand the impact of hydroxyl groups on catalytic activity, we examined the impact of sodium hydroxide on the otherwise completed Cu–TiO_2-pH7 catalyst. Specifically, the Cu–TiO_2-pH7 catalyst was immersed in a 1 M sodium hydroxide solution. After stirring for one hour, the solution was filtered, and the collected precipitate was vacuum dried at 50 °C overnight. Interestingly, we found that post-hoc exposure to a sodium hydroxide solution reduced the catalytic activity of Cu–TiO_2-pH7. The Cu–TiO_2-pH7 catalyst treated with sodium hydroxide catalysed CO conversion at a rate similar to that achieved by Cu–TiO_2-pH14. We then proceeded to measure the apparent activation energy for the four Cu–TiO_2 catalysts. As shown in Fig. 1b, CO conversion requires an activation energy (E_a) of 45.3 kJ mol^{-1} in the presence of the Cu–TiO_2-pH7 catalyst. By contrast, E_a values determined for reactions catalysed by Cu–TiO_2-pH9, Cu–TiO_2-pH14 and sodium hydroxide post-treated Cu–TiO_2-pH7 were 54.8 kJ mol^{-1}, 63.7 kJ mol^{-1} and 61.6 kJ mol^{-1}, respectively. These differences suggest that the surface hydroxyl groups are critical for achieving optimal catalytic activity.

We examined the contributions of surface hydroxyl groups to the formation of carbonate species by evaluating Cu–TiO_2 catalysts using diffuse reflectance infrared Fourier transform spectroscopy (DRIFTS). Dynamic changes in peak intensity and corresponding temperatures are shown in Fig. S3 (ESI†). We identified a band at 1540 cm^{-1} that has been associated with bicarbonates;[14] bands at 1270 cm^{-1} and 1650 cm^{-1} have been assigned to carbonate species.[17] Formates have been linked to bands located at ~1350 cm^{-1}.[17,18] Peak areas associated with individual characteristic peaks were integrated to obtain quantitative information and relative ratios of the carbon-based intermediates (Fig. 2a). Our evaluation of the Cu–TiO_2-pH7 catalyst revealed that the ratio of bicarbonate to carbonate increased with temperature and then gradually decreased at temperatures ≥120 °C. Interestingly, this ratio remains relatively constant with temperature increases in experiments performed with the Cu–TiO_2-pH14 catalyst. By contrast, the level of total bicarbonates detected in Cu–TiO_2-pH7 was initially higher than that detected in the Cu–TiO_2-pH14 catalyst. Bicarbonate loss is more rapid in response to temperature increases, largely due to the differences in bicarbonate and carbonate stability. Thus, regeneration of the active sites becomes possible. This may explain why Cu–TiO_2-pH7 is more effective at catalysing CO conversion than Cu–TiO_2-pH14. The integrated area

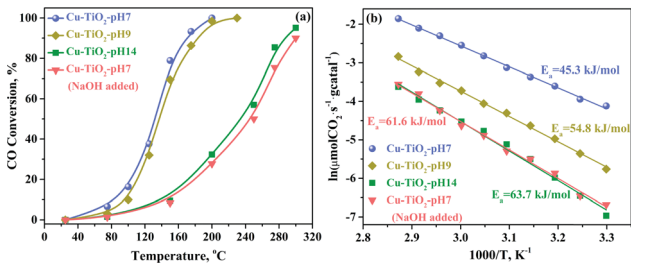

Fig. 1 (a) Light-off curves of the Cu–TiO_2 catalysts. Test conditions included 1% CO and 20% O_2/helium at a flow rate of 30 mL min^{-1}. (b) Arrhenius plots document the activation energy (E_a) required for CO oxidation in the presence of Cu–TiO_2 catalysts.

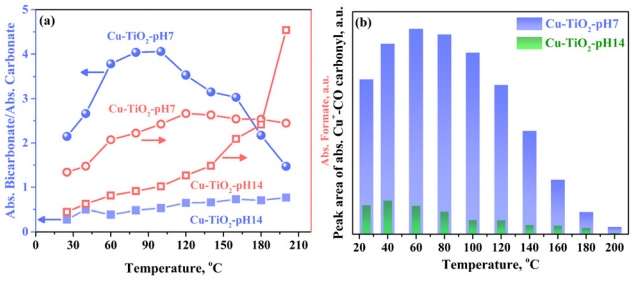

Fig. 2 (a) Ratio between the absorbance of bicarbonates and carbonates and the integrated area representing total formates as a function of temperature. (b) Integrated area of the band representing the Cu^+–CO carbonyl band at 2100–2120 cm^{-1} as a function of the reaction temperature. Catalysts examined include Cu–TiO_2-pH7 and Cu–TiO_2-pH14.

corresponding to total formates detected in both Cu–TiO_2-pH7 and Cu–TiO_2-pH14 catalysts increases with temperature. Notably, the amount of formate over Cu–TiO_2-pH14 increases when the temperature is higher than 200 °C. This increase may be explained by the positive relationship between the formation rate of formate and the pH value.[6] Given that formate species have been identified as possible intermediates in the process of CO conversion, the higher levels of formates detected in Cu–TiO_2-pH7 further confirm the greater abundance of active sites in the Cu–TiO_2-pH7 catalyst compared to the Cu–TiO_2-pH14 catalyst. The second wavenumber range featured one dominant peak at ~2100 cm^{-1} (Fig. S3, ESI†) that has been attributed to the Cu^+–CO interaction.[8,10,19] The increasing temperature led to decreased intensity in studies featuring both Cu–TiO_2-pH7 and Cu–TiO_2-pH14. However, the integrated area of the peak identified in reactions catalysed by Cu–TiO_2-pH7 was at least six times higher than the analogous peak in experiments with Cu–TiO_2-pH14 (Fig. 2b). This difference suggested that CO was favourably adsorbed by Cu–TiO_2-pH7 due to a greater abundance of active sites. The third wavelength range featured bands at ~3700 cm^{-1} in which hydroxyl groups are typically detected.[14] As a brief summary, our results revealed that residual hydroxyl groups have a significant impact on the distributions of carbonate, bicarbonate, and formate species, which could explain the differential rates of CO conversion observed.

We performed hydrogen temperature-programmed reduction (H_2-TPR) to obtain an understanding of the different copper species on the surface of each catalyst. While reduction of Cu–TiO_2-pH7 and Cu–TiO_2-pH9 was detected at 60 °C, the dominant reaction was observed below 120 °C. The results of deconvolution analysis revealed three specific reduction peaks. The first reduction peak (Peak I) may be related to either surface oxygen[20] or highly-dispersed copper species located at the Cu–Ti interface.[21] The second and third reduction peaks (Peak II and Peak III) contributed to the overall absence of peak-shape symmetry; this finding may be the result of step-wise reductions of copper(II) oxides.[22] Subsequent calculations revealed that the amounts of consumed hydrogen that are indicative of a step-reduction process decreased slightly from 83% for Cu–TiO_2-pH7 to 80% for Cu–TiO_2-pH9 (Fig. 3a). This finding may explain why Cu–TiO_2-pH7 and Cu–TiO_2-pH9 exhibit similar catalytic efficiencies in the low-temperature range. For Cu–TiO_2-pH14, the reduction reaction did not begin until 100 °C, and the majority of the reduction took place at a higher temperature range. Our calculations revealed that 36% of hydrogen consumption (percentages of Peak II and Peak III) occurred at temperatures >125 °C. These high-temperatures may be needed to reduce crystalline copper oxide.[23] Our results of H_2-TPR revealed that the copper species on the surface of the catalyst exhibit different morphologies and oxidation states. Thus, we anticipate that the types and concentrations of surface oxygen species may also be different.

To examine the differences among surface oxygen species, CO temperature programmed surface reaction (CO-TPSR) was applied, and the production of carbon dioxide was monitored. The results of peak deconvolution analysis suggested that different types of surface oxygen species existed at the various temperature ranges. Low and medium-temperature oxygen species (Peak I and Peak II) are dominant over both Cu–TiO_2-pH7 and Cu–TiO_2-pH9 catalysts (Fig. 3b). While the percentage

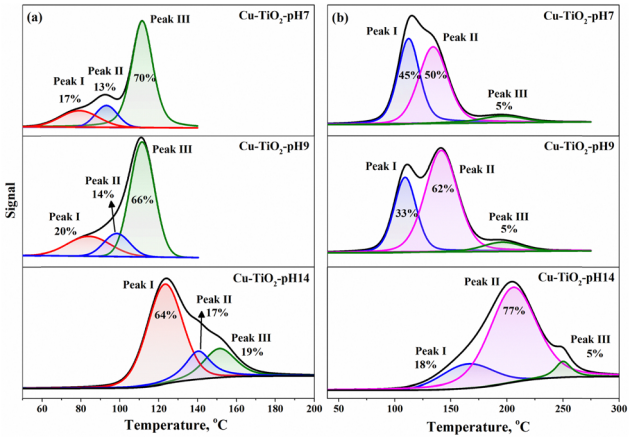

Fig. 3 (a) Hydrogen-temperature programmed reduction (H_2-TPR) and (b) carbon monoxide temperature-programmed surface reaction (CO-TPSR) profiles. Catalysts examined include Cu–TiO_2-pH7, Cu–TiO_2-pH9, and Cu–TiO_2-pH14.

areas representing low and medium-temperature oxygen species varied with the concentration of surface hydroxyl groups, nearly 95% of the total oxygen species was detected at temperatures <150 °C. The presence of these oxygen species correlated with the high levels of activity of these catalysts within the lower temperature range. High-temperature oxygen species (Peak III) contributed to 5% of the overall reduction catalysed by Cu–TiO_2-pH7 and Cu–TiO_2-pH9. By contrast, surface oxygen species were detected primarily at temperatures >150 °C in reactions featuring Cu–TiO_2-pH14. Although Peak I and Peak II associated with Cu–TiO_2-pH14 were larger than Peak III, they appeared only at temperatures >150 °C. By contrast, both Peak I and Peak II associated with the Cu–TiO_2-pH7 and Cu–TiO_2-pH9-catalysed reactions were detected at temperatures <150 °C. Our results from TPR analysis using hydrogen and CO as probe molecules confirmed the existence of different active sites on the catalyst surface. Catalysts obtained from solutions at pH 7 or pH 9 exhibit more active sites than catalysts generated from solutions at pH 14.

We also used X-Ray photon spectroscopy (XPS) to explore the oxidation state of copper species and to identify the types of oxygen species involved in this reaction. The spectra were deconvoluted into three pairs of peaks with each corresponding to a different copper oxidation state (Fig. S4, ESI†). We analysed the percentages of Cu^+ and Cu^{2+}, which are the two oxidation states at the highest concentrations in Cu–TiO_2 catalysts. Our results revealed an increase in the relative ratios of Cu^+/Cu^{2+} that paralleled the increase in residual hydroxyl species detected in the Cu–TiO_2 catalysts. The results shown in Fig. 4 documented a relative surface concentration of Cu^+ species of 30% in the Cu–TiO_2-pH14 catalyst; this percentage is higher than that detected in either of the other Cu–TiO_2 catalysts. However, the relative surface concentration of Cu^{2+} species in the Cu–TiO_2-pH7 catalyst was 77%. The main O 1s peak gradually shifted from 529.5 eV to 529.1 eV in response to an increase in pH (Fig. S4, ESI†). Meanwhile, the peak at 531.6 eV was attributed to bridging surface hydroxyl groups.[8] The results

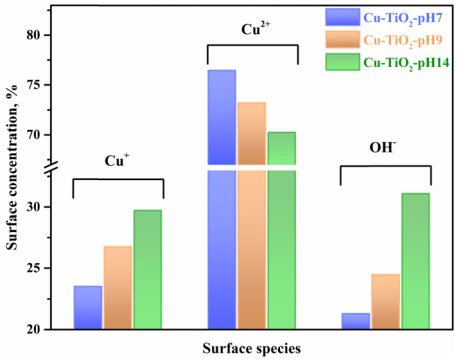

Fig. 4 Concentrations of copper and oxygen species on the catalyst surface based on the XPS spectra of Cu 2p and O 1s. Catalysts used in these experiments include Cu–TiO_2-pH7, Cu–TiO_2-pH9, and Cu-TiO_2-pH14.

shown in Fig. 4 document the larger fraction of the area encompassed by the 531.6 eV peak. This finding is consistent with the fact that the Cu–TiO_2-pH14 catalyst was prepared from a solution at higher pH.

It is important to note that our approach to the synthesis of Cu–TiO_2 catalysts provides a direct platform that can be used to examine the roles of active and bystander species. Conventionally, a calcination step was required to generate copper oxides. A pre-treatment step was also included to further optimise activity. The use of these variations and optimisations can complicate our understanding of the specific contributions of localised species to the generation of active sites and how effectively they participated in the reduction. This may explain why most of the previous work on this subject focused only on correlations between a single copper species and the reaction rate.[2,3] If we followed this traditional perspective and correlated catalytic activity with the concentration of Cu^+ or Cu^{2+} alone, we are assuming that one copper species provides the major contributions to an otherwise complex reaction system. As being discussed previously,[8,14,15] we need to acknowledge the contributions of the local environment of these copper species, besides their oxidation states, because these species may also have an impact on catalytic performance. For example, results from previous reports suggested that Ti^{3+} might facilitate the formation of Cu^+ through a redox reaction between Cu^{2+} and Ti^{3+}.[10,24] Here, in addition to varied Cu^+ and Cu^{2+} concentrations, we also detected different concentrations of surface hydroxyl groups. Our results suggest that it is both reasonable and important to consider the impact of surrounding hydroxyl groups as part of the overall structure–activity relationship. We chose 932.4 eV as the characteristic energy of Cu^+ species. We obtained quantitative information from the surface hydroxyl groups based on the peak identified at 531.6 eV. The ratio of $[Cu^+]/[OH^-]$ was determined based on values from integrated XPS peaks. Ratios of 1.10, 1.09, and 0.96 were calculated for Cu–TiO_2-pH7, Cu–TiO_2-pH9, and Cu–TiO_2-pH14, respectively (Table 1). We also determined the reaction rate based on the formation of carbon dioxide. We identified reaction rates (in the unit of $\mu mol\ s^{-1}\ gcatal^{-1}$) of 0.16, 0.06, and 0.03 for Cu–TiO_2-pH7, Cu–TiO_2-pH9, and Cu–TiO_2-pH14, respectively (Table 1). These data indicate that the reaction rates increased in parallel with increases in the concentrations of copper(I) and hydroxyl groups. Collectively, our results suggest that all elements contributing to this process have a specific impact on individual reaction domains.

The synthesis of Cu–TiO_2 *via* a direct reaction between copper acetate and sodium hydroxide enabled us to explore a role for localised hydroxyl groups in directing the oxidation of carbon monoxide. Our results suggest that while the surface abundance of copper(I) species is a critical factor, the ratio of copper(I) to surface hydroxyl groups should also be considered when it comes to optimizing the reaction rate.

The authors appreciate the support provided by the University of New Hampshire and the Summer Teaching Assistant Fellowship (to G. C.).

Data availability

The data supporting this article have been included as part of the ESI.†

Conflicts of interest

There are no conflicts to declare.

Notes and references

1 G. Wu, N. Guan and L. Li, *Catal. Sci. Technol.*, 2011, **1**, 601–608.
2 J. Szanyi and D. W. Goodman, *Catal. Lett.*, 1993, **21**, 165–174.
3 G. G. Jernigan and G. A. Somorjai, *J. Catal.*, 1994, **147**, 567–577.
4 A. J. Maynes, D. M. Driscoll, P. A. DeSario, J. J. Pietron, A. M. Pennington, D. R. Rolison and J. R. Morris, *J. Phys. Chem. C*, 2020, **124**, 21491–21501.
5 W. Liu and M. Flytzani-Stephanopoulos, *Chem. Eng. J. Biochem. Eng. J.*, 1996, **64**, 283–294.
6 A. Adamu, M. Isaacs, K. Boodhoo and F. R. Abegão, *J. CO_2 Util.*, 2023, **70**, 102428.
7 M. Fracchia, P. Ghigna, T. Pozzi, U. Anselmi-Tamburini, V. Colombo, L. Braglia and P. Torelli, *J. Phys. Chem. Lett.*, 2020, **11**, 3589–3593.
8 G. Cao, N. A. Deskins and N. Yi, *Appl. Catal., B*, 2021, **285**, 119748.
9 P. H. Matter and U. S. Ozkan, *J. Catal.*, 2005, **234**, 463–475.
10 G. Cao and N. Yi, *Catal. Commun.*, 2022, **170**, 106484.
11 X. Zhang, H. Li, Y. Yang, T. Zhang, X. Wen, N. Liu and D. Wang, *J. Environ. Chem. Eng.*, 2017, **5**, 5179–5186.
12 C. Bilanin, Y. K. Zheng, A. Vidal-Moya, E. Pardo, M. Mon and A. Leyva-Pérez, *Mol. Catal.*, 2024, **553**, 113786.
13 N. Antil, M. Chauhan, N. Akhtar, R. Kalita and K. Manna, *J. Am. Chem. Soc.*, 2023, **145**, 6156–6165.
14 A. Davó-Quiñonero, M. Navlani-García, D. Lozano-Castelló, A. Bueno-López and J. A. Anderson, *ACS Catal.*, 2016, **6**, 1723–1731.
15 G. Cao and N. Yi, *New J. Chem.*, 2020, **44**, 14781–14785.
16 T. Kida, T. Oka, M. Nagano, Y. Ishiwata and X. G. Zheng, *J. Am. Ceram. Soc.*, 2007, **90**, 107–110.
17 C. Ma, C. Yang, B. Wang, C. Chen, F. Wang, X. Yao and M. Song, *Appl. Catal., B*, 2019, **254**, 76–85.
18 A. Martínez-Arias, A. B. Hungría, G. Munuera and D. Gamarra, *Appl. Catal., B*, 2006, **65**, 207–216.
19 M. M. Wang, J. Yu, W. W. Wang, J. X. Chen, C. J. Jia and R. Si, *J. Phys. Chem. C*, 2020, **124**, 25270–25281.
20 D. Chen, D. He, J. Lu, L. Zhong, F. Liu, J. Liu, J. Yu, G. Wan, S. He and Y. Luo, *Appl. Catal., B*, 2017, **218**, 249–259.
21 W. W. Wang, P. P. Du, S.-H. Zou, H. Y. He, R. X. Wang, Z. Jin, S. Shi, Y. Y. Huang, R. Si, Q. S. Song, C. J. Jia and C. H. Yan, *ACS Catal.*, 2015, **5**, 2088–2099.
22 W. Yang, L. Li, Y. Fang, Y. Shan, J. Xu, H. Shen, Y. Yu, Y. Guo and H. He, *Catal. Sci. Technol.*, 2020, **10**, 1661–1674.
23 R. Si, J. Raitano, N. Yi, L. Zhang, S.-W. Chan and M. Flytzani-Stephanopoulos, *Catal. Today*, 2012, **180**, 68–80.
24 C. S. Chen, T. C. Chen, C. C. Chen, Y. T. Lai, J. H. You, T. M. Chou, C. H. Chen and J. F. Lee, *Langmuir*, 2012, **28**, 9996–10006.

